JACS
JOURNAL OF THE AMERICAN CHEMICAL SOCIETY
pubs.acs.org/JACS
Article

Optimizing Hydrogen Storage in MOFs through Engineering of Crystal Morphology and Control of Crystal Size

Kuthuru Suresh, Darpandeep Aulakh, Justin Purewal, Donald J. Siegel, Mike Veenstra, and Adam J. Matzger*

Cite This: J. Am. Chem. Soc. 2021, 143, 10727−10734
Read Online
ACCESS | Metrics & More | Article Recommendations | Supporting Information

ABSTRACT: Metal−organic frameworks (MOFs) are promising materials for hydrogen storage that fail to achieve expected theoretical values of volumetric storage density due to poor powder packing. A strategy that improves packing efficiency and volumetric hydrogen gas storage density dramatically through engineered morphologies and controlled-crystal size distributions is presented that holds promise for maximizing storage capacity for a given MOF. The packing density improvement, demonstrated for the benchmark sorbent MOF-5, leads to a significant enhancement of volumetric hydrogen storage performance relative to commercial MOF-5. System model projections demonstrate that engineering of crystal morphology/size or use of a bimodal distribution of cubic crystal sizes in tandem with system optimization can surpass the 25 g/L volumetric capacity of a typical 700 bar compressed storage system and exceed the DOE targets 2020 volumetric capacity (30 g/L). Finally, a critical link between improved powder packing density and reduced damage upon compaction is revealed leading to sorbents with both high surface area and high density.

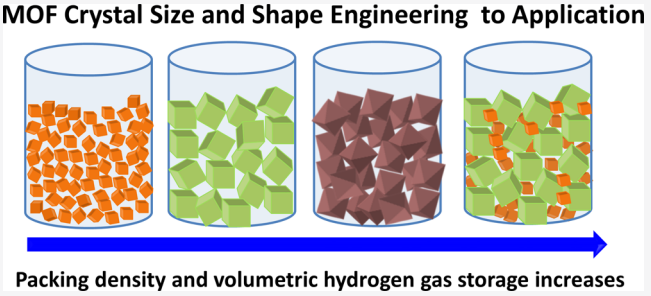

INTRODUCTION

The storage of sufficient quantities of fuel on automobiles presents one of the greatest challenges to realizing a hydrogen economy. A number of technologies have been pursued for improving the energy density of hydrogen; these are divided into physical-based (cold or cryo- compressed hydrogen storage) and materials-based (chemical hydrogen storage materials and metal hydrides, sorbents) approaches.[1−5] Storage in metal−organic framework (MOF) sorbents via adsorption presents one of the most promising approaches due to fast charge/discharge kinetics, facile reversibility, and high gravimetric capacities.[6] However, high volumetric densities are uncommon in MOFs, and these densities can be impacted by multiple factors such as MOF structure, the nature of the interaction of H_2 with the MOF, and the packing of the MOF material.[7] The issue of materials packing, although acknowledged as an important factor, has not been widely examined.

Calculations of volumetric performance often assume (unrealistic) single crystal packing densities, and it must be recognized that this represents an upper limit to performance. Analysis by the Hydrogen Storage Engineering Center of Excellence (HSECoE) demonstrated that inefficient material packing can result in a >60% volumetric density reduction compared to the single crystal.[6] In other words, volumetric performance of the MOF in a real system will be profoundly impacted by the discrepancy between MOF material packing density and crystallographic density. Consequently, improvements to the intrinsic capacity of the adsorbent, which have been the focus of materials research for more than a decade, can be "undone" by poor packing of the media in the storage system. Therefore, MOF packing efficiency is an important parameter and plays a critical role in improving volumetric hydrogen storage density in real systems.

The packing of uniform spheres has an upper limit of 74% packing efficiency.[8] Achievement of this threshold requires an ordered arrangement in space, and it has recently been shown that the random packing of spheres cannot exceed 63% packing efficiency.[8] For other particle shapes, the results differ: randomly jammed tetrahedral dice[9] exhibit packing efficiencies of 76% compared to 100% packing efficiency for the regularly arranged platonic solids. However, there exists no theoretical framework for predicting the minimum void space that is practically achievable for polydisperse shapes characteristic of MOFs. Thus, packing density studies on real MOF samples whose crystals exhibit different shapes and sizes are currently the best pathway to understand packing efficiency. Unfortunately, strategies to engineer crystal shape/size properties and

Received: May 12, 2021
Published: July 9, 2021

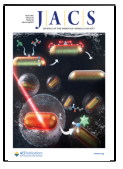

https://doi.org/10.1021/jacs.1c04926
J. Am. Chem. Soc. 2021, 143, 10727−10734

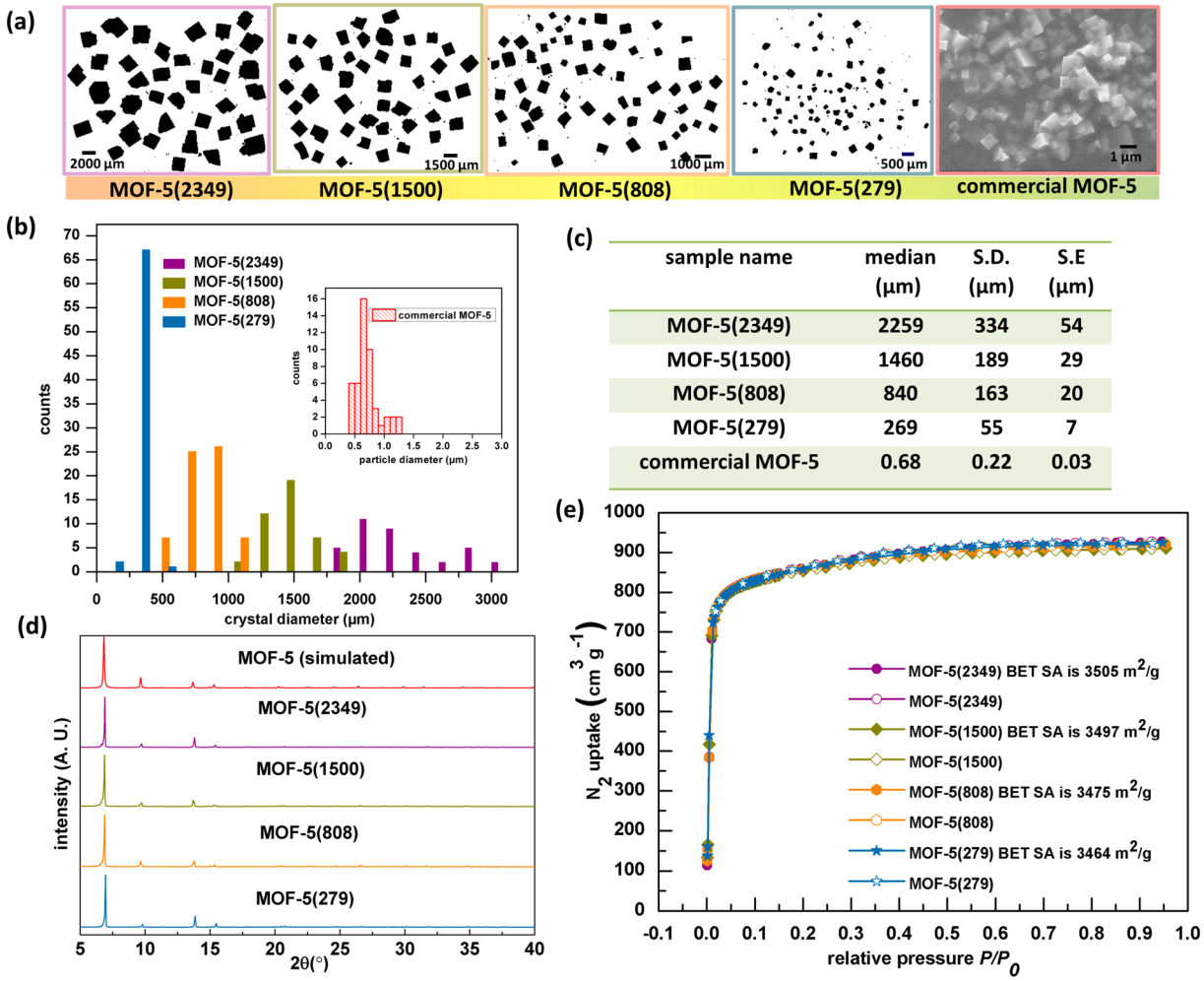

sample name	median (μm)	S.D. (μm)	S.E (μm)
MOF-5(2349)	2259	334	54
MOF-5(1500)	1460	189	29
MOF-5(808)	840	163	20
MOF-5(279)	269	55	7
commercial MOF-5	0.68	0.22	0.03

Figure 1. (a) Thresholded optical images of four different crystal sizes and SEM image for commercial MOF-5 crystallites. (b) and (c) Histogram plot (inset histogram plot for commercial MOF-5) and tabulated crystal size distributions range and median values with standard deviation (S.D.) and standard error (S.E.) for four different crystal sizes and commercial MOF-5 samples. (d) PXRD patterns of four crystal sizes samples compared with the simulated pattern of MOF-5 computed from the crystal structure (refcode SAHYOQ). (e) N_2 sorption isotherms of four crystal sizes (adsorption data are shown with filled symbols while desorption data are shown with empty symbols).

pack MOFs with low void fraction have not been widely explored. Here, MOFs with targeted crystal shapes (cubic, cuboctahedral, octahedral, and spherical) and sizes are synthesized. Their packing density and hydrogen uptake are characterized and compared with BASF-produced (hereafter "commercial") material. The optimization of crystal size and engineering of crystal morphology for MOF-5 is demonstrated to dramatically improve volumetric hydrogen storage performance, both in terms of packing density (up to 100% improvement) and compacted density (up to 33%), with respect to what can be achieved with commercial MOF-5 powders.

RESULTS AND DISCUSSION

To assess the influence of crystal size and shape on packing efficiency, the benchmark compound MOF-5 was selected as a model.[10] MOF-5 shows one of the highest deliverable hydrogen volumetric capacities among all MOFs based on its single crystal density[11] and, based on techno-economic analysis, can meet adsorbent cost targets.[12] Nevertheless, the poor packing density of MOF-5 limits its volumetric hydrogen capacity in practice.[11,13] In the present study, cubic MOF-5 crystals with four different sizes, varying from hundreds of micrometers to millimeter scale, are obtained by modulating the metal:ligand (M:L) molar ratio as well as the reactant concentration. In addition, new methods for synthesizing MOF-5 crystals with different shapes by the action of additives are described. Controlling these aspects of MOF crystals is demonstrated to dramatically improve volumetric hydrogen storage performance. It is anticipated that these lessons are directly applicable to the large family of cubic MOFs existing in the literature.

CONTROL OF CRYSTAL SIZE

The effect of synthetic process parameters such as concentration of reagents, temperature, and time were investigated for their effect on crystal size and size distribution. Reactions for shorter duration (12 to 18 h) at high temperature (110 to 150 °C) afforded cubic crystals with a broad size distribution (on the order of 200−1300 μm). Longer durations (24 to 72 h) at lower temperatures (60 to 90 °C) yielded crystals with narrow size distributions but led to a greater than 15% reduction in BET surface area. The optimal conditions for narrowing the size distribution without compromising surface area were 18−

https://doi.org/10.1021/jacs.1c04926
J. Am. Chem. Soc. 2021, 143, 10727−10734

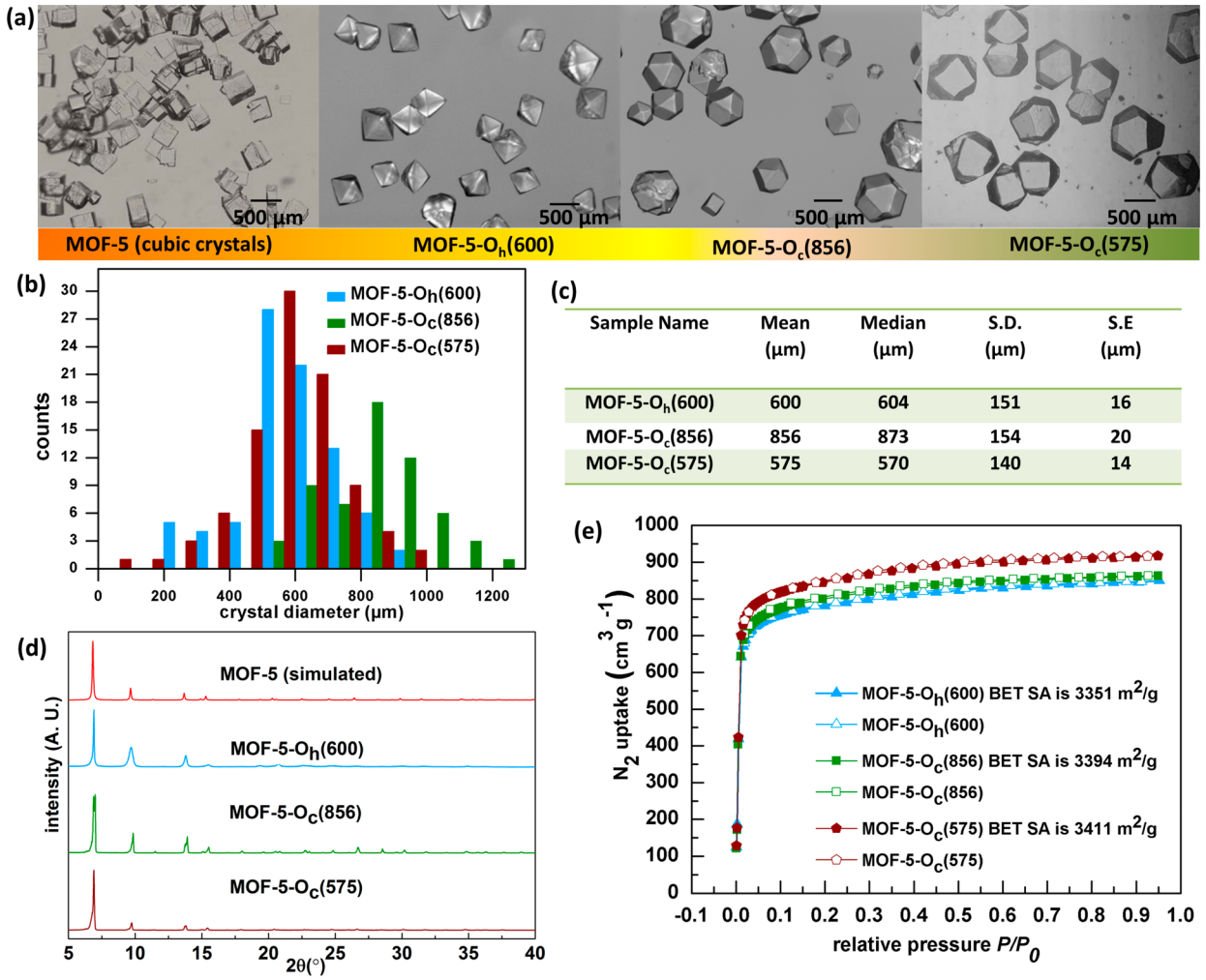

Sample Name	Mean (μm)	Median (μm)	S.D. (μm)	S.E (μm)
MOF-5-O_h(600)	600	604	151	16
MOF-5-O_c(856)	856	873	154	20
MOF-5-O_c(575)	575	570	140	14

Figure 2. (a) Optical images of MOF-5 crystals with controlled morphologies. (b) and (c) Histogram plot and tabulated crystal size distributions range and median values for different morphologies of MOF-5. (d) PXRD patterns of new MOF-5 morphologies compared with the simulated pattern of MOF-5 computed from the crystal structure (refcode SAHYOQ). (e) N_2 sorption isotherms for different morphologies of MOF-5 (adsorption data are shown with filled symbols while desorption data are shown with empty symbols).

24 h at 100 °C. Variation of the metal:ligand (M:L, $Zn(NO_3)_2.6H_2O$:H_2BDC) molar ratio was studied over the range of 1:1 to 5:1. For samples with M:L = 1 or M:L ≥ 4, the final product had an additional solid phase other than MOF-5. Accordingly, efforts were focused on 1 < M:L < 4. Additionally, the reactant concentration was varied to tune crystal size distributions.

Eventually, the optimized M:L molar ratio mixtures (3.8:1, 2.3:1, 1.7:1, and 1.7:1(2-fold dilution) were heated at 100 °C for 24 h. These four recipes resulted in four different crystal size distributions: MOF-5(2349), MOF-5(1500), MOF-5(808), and MOF-5(279), respectively, where the number in parentheses indicates the mean crystal size in microns (Figure 1a, Supporting Information). The crystal sizes of all samples and their distributions and statistics are represented in Figure 1b,c. The crystal sizes of these samples were compared to commercial MOF-5 (Figure 1a) which has a submicron average crystal size. Phase purity of all samples was confirmed through powder X-ray diffraction, and it was observed that powder patterns of all samples agree with the calculated pattern of MOF-5 simulated from the crystal structure (Figure 1d). All samples exhibit very good surface areas (3505−3464 m^2/g) matching the expected theoretical surface area (3563 m^2/g) of MOF-5 (Figure 1e).

MORPHOLOGY ENGINEERING

Inspired by observations of different morphologies of MOF-5 by the action of a tricarboxylic acid linker,[13] we conjectured that carboxylic acids can serve as additives for synthesizing new morphologies. An array of di-, tri-, and tetra-topic carboxylic acids were examined as morphology modifiers (Figure S1, Supporting Information); the role of additive concentration in influencing morphology by varying the additive molar ratio while keeping the ratio of BDC and $Zn(NO_3)_2.6H_2O$ (1:2.8 molar ratio) unchanged was also examined (Supporting Information).

Ditopic Carboxylic Acid (H_2L) Linkers. Several alkane dicarboxylic acids including oxalic acid, malonic acid, succinic acid, glutaric acid, adipic acid, and suberic acid were tested for their ability to modify morphology when employed as additives at the 5−10 mol % level. It was observed that introducing these carboxylic acids to the MOF-5 reaction mixture afforded no change in MOF-5 cubic crystal morphology. It is known that some linear (aromatic) linkers can give rise to new phases

https://doi.org/10.1021/jacs.1c04926
J. Am. Chem. Soc. 2021, 143, 10727−10734

Scheme 1. Schematic Representation of Crystal Growth Mechanism for All Three Morphologies of the MOF-5[a]

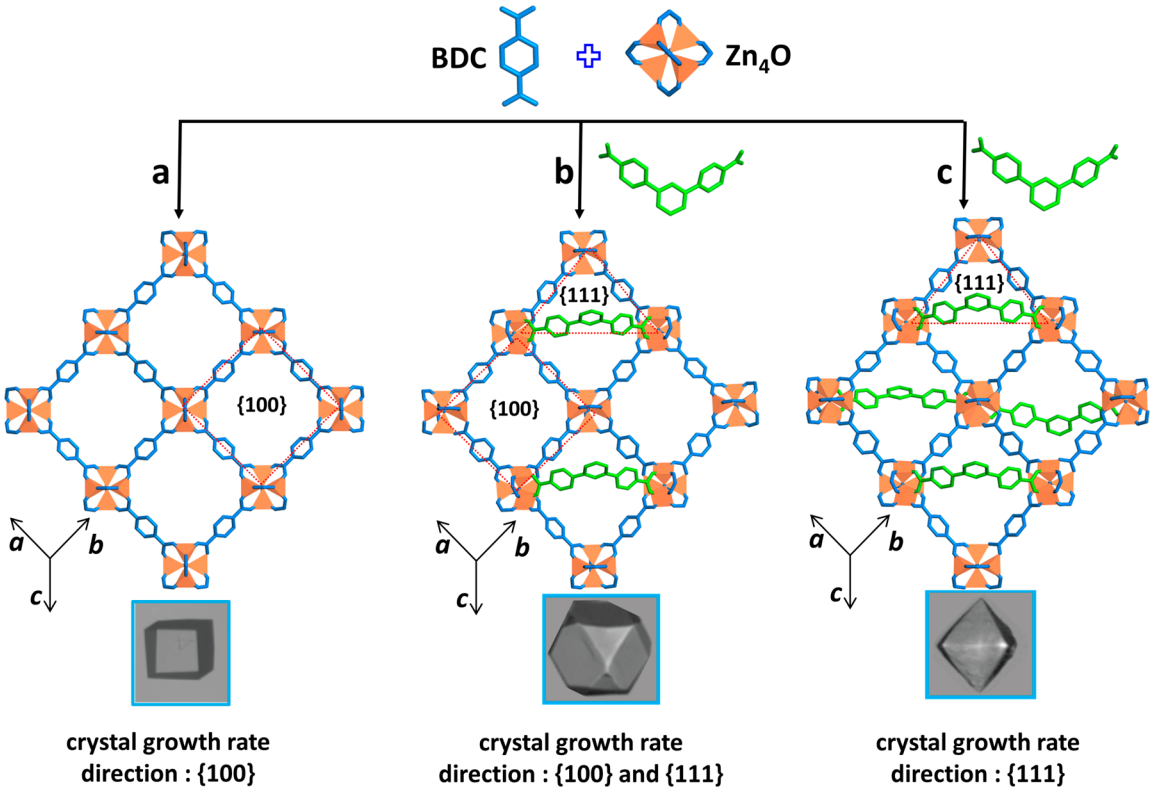

[a]The cubic crystal morphology (a) is controlled by the slower crystal growth rate along {100} facet direction. The additive (*m*-terephenyl-4,4′-dicarboxylate shown in green) blocks MOF-5 growth along the {111} direction partially or totally at the expense of all {100} facets during crystal growth which results in the formation of cuboctahedral (b) and octahedral (c) crystal morphologies, respectively.

incorporating zinc and two linkers,[14] but in all the cases examined here, the predominant phase was MOF-5.

Tritopic Carboxylic Acid (H_3L) Linkers. Four tritopic carboxylic acids (trimesic acid, [1,1′-biphenyl]-3,4′,5-tricarboxylic acid, 1,3,5-tris(4-carboxyphenyl)benzene (H_3BTB) and 2,4,6-tris(4-carboxyphenyl)aniline (NH_2−H_3BTB)) were screened. Among these, the addition of H_3BTB and NH_2−H_3BTB to the initial MOF-5 reagent mixture were observed to generate different shaped crystals. When ∼4 mol % H_3BTB was added to the MOF-5 reaction mixture and heated at 100 °C for 24 h, uniform octahedral (O_h) morphology crystals (MOF-5-O_h(600)) are synthesized, while the addition of lower amounts of H_3BTB (∼2 mol %) to the MOF-5 reaction mixture at 100 °C for 48 h yielded uniform cuboctahedral (O_c) shaped crystals (MOF-5-O_c(856)). The addition of H_3BTB at concentrations greater than ∼4 mol % resulted in both needle- and octahedral-shaped crystals which is consistent with a mixed linker MOF where the needles correspond to UMCM-1.[15,16] Similarly, the addition of NH_2−H_3BTB (∼3 mol %) to the reaction mixture at 100 °C for 24 h resulted in cuboctahedral shaped crystals (MOF-5-O_c(575)). Addition of this additive in higher mol % resulted in the final product having an additional crystalline solid phase other than MOF-5 as well as a greater than 15% reduction in BET surface area.

The obtained new morphologies (MOF-5-O_h(600), MOF-5-O_c(856), and MOF-5-O_c(575) where the number indicates the mean crystal size in microns) and their crystal size distributions and statistics are represented in Figure 2a−c). PXRD patterns of these noncubic morphologies are consistent with the pattern for MOF-5 simulated from the single crystal X-ray structure (Figure 2d). This reveals that the overall framework structure remains unchanged signaling the ability of additives to engineer morphology without substantially changing crystal structure. All samples (MOF-5-O_h(600), MOF-5-O_c(856), and MOF-5-O_c(575)) exhibit a small reduction (at most ∼150 m^2/g) in BET surface area compared to optimal cubic MOF-5 (Figure 1e).

Tetratopic Carboxylic Acid (H_4L) Linkers. Tetratopic (5′-((3,5-dicarboxyphenyl)ethynyl)-[1,1′:3′,1″-terphenyl]-4,4″-dicarboxylic acid and 5′-(4-carboxyphenyl)-[1,1′:3′,1″-terphenyl]-3,4″,5-tricarboxylic acid) carboxylic acids added to the initial MOF-5 reagent mixture generated different cuboctahedral, octahedral, and spherical shaped crystals in 24 h at 100 °C respectively (Figure S3a, Supporting Information). The PXRD patterns of these samples demonstrate that they are MOF-5 (Figure S3b, Supporting Information). However, with these new morphologies, reproducibility is a major issue and a greater than 15% reduction in BET surface area was observed making them unsuitable for hydrogen storage.

MECHANISM OF CRYSTAL MORPHOLOGY ENGINEERING

To understand the evolution of MOF-5 morphologies in the presence of additives, the relative growth rates of the different surface facets of the crystal must be accounted for. Changing reagent concentration, the presence of additives, and/or modulation of synthesis conditions can suppress the growth rate of certain crystallographic facets. Regardless of changes made to the relative concentrations of reagents (M:L molar ratio), temperature, and reaction time for MOF-5 synthesis,

https://doi.org/10.1021/jacs.1c04926
J. Am. Chem. Soc. 2021, 143, 10727−10734

cubic morphology crystals with {100} crystallographic facets were consistently obtained. This indicates that slow crystal growth occurs along the {100} facet (Scheme 1a).

By contrast, H_3L or H_4L additives significantly alter the relative growth rates of crystal facets, resulting in different crystal morphologies. Among (H_3L or H_4L) additives, only those containing a *m*-terephenyl-4,4′-dicarboxylic acid moiety resulted in noncubic morphologies. We hypothesize that the *m*-terephenyl-4,4′-dicarboxylic acid moiety is responsible for the formation of the modified crystal morphology because it can bridge two Zn_4O clusters situated diagonally across a pore window in the (100) plane of MOF-5[3] (oxo-oxo length of 18.303 Å). The notion that a *m*-terephenyl-4,4′-dicarboxylate can bridge this distance is supported by inspection of the MOF-177[17] structure; the closest distance between Zn_4O units in this MOFs is 18.432 Å and these are bridged by *m*-terephenyl-4,4′-dicarboxylate units of 1,3,5-tris(4-benzoate)-benzene. Thus, during the initial stage of crystal growth, the additive containing the *m*-terephenyl-4,4′-dicarboxylic acid moiety (Scheme 1) blocks MOF-5 growth along the {111} facet direction which results in a slow growth rate of this facet and expression of this crystal surface. This additive blocks the {111} facet direction accompanied by the comparable growths rate of both {100} and {111} facets on the crystal surface when the modulator is at low concentrations. Therefore, cuboctahedral shaped crystals covered by six {100} and eight {111} facets are observed (Scheme 1b). At higher additive concentrations, MOF-5 growth along the {111} facet direction is blocked at the expense of all regularly observed {100} facets resulting in the formation of octahedral crystal morphology entirely covered by eight {111} facets (Scheme 1c). In contrast, additives lacking the *m*-terephenyl-4,4″-dicarboxylic acid motif are larger or smaller than the cluster spacing on the MOF-5 {111} facet and accordingly these additives do not yield new morphologies. These morphological transitions clearly demonstrate that employing additives that selectively interact with certain crystallographic facets and varying their concentration can change the relative growth rate of different crystallographic facets to control morphology and provides a designed way to control morphology that complements approaches based on surfactants.[18,19]

PACKING DENSITY

In hydrogen storage applications it is desirable to fill the storage vessel with sorbent in a manner that minimizes the presence of voids and thereby maximizes the volumetric density. The packing density for all samples was optimized and measured using a jolting volumeter (see experimental details in Supporting Information). The number of taps vs packing density for commercial MOF-5, size-controlled MOF-5 (MOF-5(2349), MOF-5(1500), MOF-5(808), and MOF-5(279)), and controlled crystal morphology (MOF-5-O_h(600), MOF-5-O_c(856), and MOF-5-O_c(575)) samples was monitored. Packing density increases with increasing number of taps until it converges to a constant value (Figure 3). It was observed that all samples exhibit a notable improvement in packing density of (63% to 93%) compared to commercial MOF-5 (Table 1). Additionally, the packing density of a mixture of size-controlled of MOF-5(2349) and MOF-5(808) in a 7:1 mass ratio[20] displays a remarkable (100%) improvement over commercial MOF-5. All newly synthesized size-controlled cubic and noncubic morphology crystals possess low external surface area that allows the larger

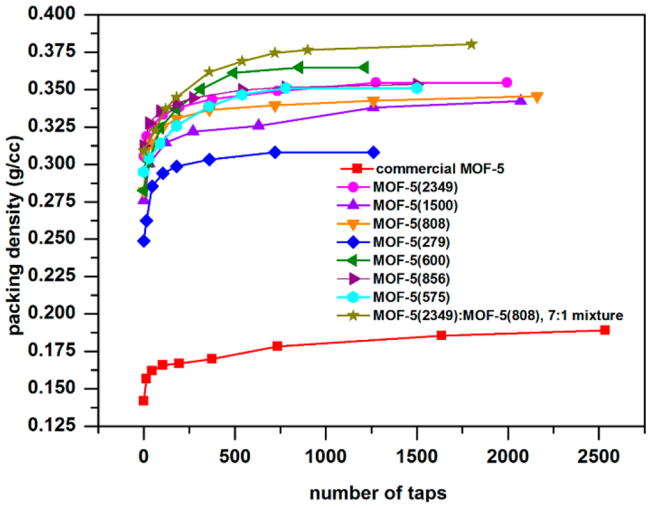

Figure 3. Representative packing density measurements of MOF-5 cubic size-controlled, and different noncubic crystal morphology samples.

Table 1. Representative Packing Density Improvement for MOF-5 Cubic Size-Controlled, and Different Non-Cubic Crystal Morphology Samples Compared to Commercial MOF-5

sample name	packing density (g/cm^3)	improvement over commercial MOF-5 (in %)
commercial MOF-5	0.189	
MOF-5(2349)	0.355	87
MOF-5(1500)	0.342	81
MOF-5(808)	0.346	83
MOF-5(279)	0.308	63
MOF-5-O_h(600)	0.365	93
MOF-5-O_c(856)	0.353	87
MOF-5-O_c(575)	0.352	86
MOF-5(2349):MOF-5(808), 7:1 mixture	0.380	100

size crystals to flow more easily. Consequently, these samples becomes more compact upon tapping when compared to small crystallite sample of commercial MOF-5, which exhibits high external surface area with more cohesive behavior impeding free flow of crystals.[21,22] Empirically, noncubic crystal morphology samples (MOF-5-O_h(600), MOF-5-O_c(856), and MOF-5-O_c(575)) have less electrostatic charge than cubic MOF-5 samples and are relatively free-flowing leading to the greater individual packing densities. However, in a practical storage system, some degree of mechanical compaction may be used to further increase capacity beyond powder density. It is presently uncertain if the improvements in powder density demonstrated here can translate to improvements after densification.

COMPACTION STUDY

Hydrogen gas storage measurements were performed for commercial MOF-5, size-controlled MOF-5, a bimodal mixture of MOF-5(2349) and MOF-5(808), and octahedral crystal morphology samples to quantify the influence of mechanical compaction on the hydrogen adsorption capacity at 77 K. Compaction represents an approach to further densify materials beyond the observed tap densities albeit with the risk of structural damage due to high contact pressures. Selected

https://doi.org/10.1021/jacs.1c04926
J. Am. Chem. Soc. 2021, 143, 10727−10734

measurements are provided in Figure S6, Supporting Information, which demonstrate the excess hydrogen adsorption isotherms after compacting samples to successively higher densities. The commercial MOF-5 and size-controlled MOF-5 (MOF-5(2349), MOF-5(1500), MOF-5(808), and MOF-5(279)) samples retain greater than 95% of their excess gravimetric hydrogen capacity up to a compaction density fraction (packing density/crystal density) of between 57 and 70%; thereafter, their hydrogen capacity decreases with increasing compaction density of the sample (Figure 4)

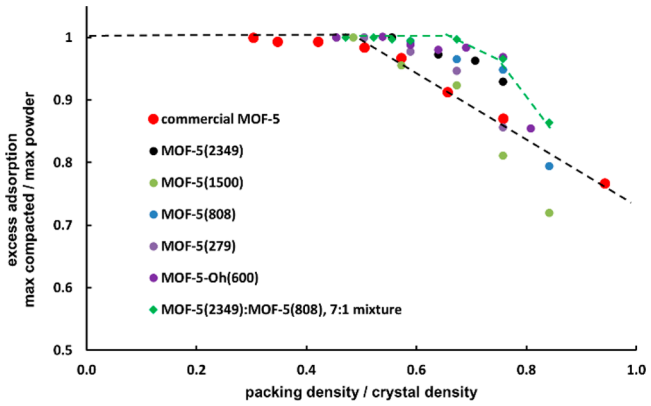

Figure 4. Excess adsorption of hydrogen gas vs compaction density. The *x*-axis corresponds to the density of the compacted MOF-5 sample divided by its crystal density (0.594 g/cm^3[24]). The *y*-axis corresponds to the ratio between the maximum excess hydrogen adsorption at 77 K for a MOF-5 sample compacted to a specific density by the value for the initial value measured for the MOF-5 sample.

consistent with structural damage.[22] By contrast, the size-controlled MOF-5 bimodal mixture of MOF-5(2349) and MOF-5(808) in a 7:1 mass ratio and MOF-5-O$_h$(600) samples retain high gravimetric capacity up to compaction density of approximately 75% vs excess hydrogen gas adsorption. Importantly, the compaction density for MOF-5(2349), MOF-5(1500), MOF-5(808) and MOF-5(279), 7:1 mixture, and MOF-5-O$_h$(600) samples exhibit improvements over the compacted density of commercial MOF-5 with negligible performance loss, respectively. The 7:1 mixture resulted in the most notable density improvement of 33% when comparing the inflection point from the commercial MOF-5 to maintain powder adsorption performance (green dashed vs black dashed trend lines).[23] This result indicates that an improvement in powder density results in less damage upon compaction, presumably due to the presence of an optimized arrangement of crystals (see Table S5, Supporting Information). Any percentage gain in volumetric capacity from the density improvement is a direct gain in driving range contributing to a projected system that can exceed the performance of the current state-of-the art 700 bar compressed gas system in tandem with system engineering improvements as shown in Figure 5.

STORAGE SYSTEM PROJECTIONS

The correlation between material level and system-level volumetric hydrogen capacities is represented in Figure 5. The HSECoE adsorbent system model used for these system predictions takes as input MOF material properties and as output predicts the system characteristics of a full scale 5.6 kg

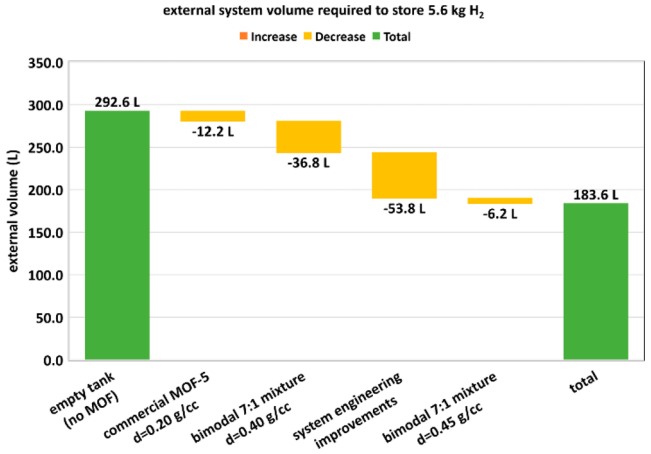

Figure 5. Waterfall chart depicting the total external system volume of bimodal MOF-5(2349):MOF-5(808), 7:1 mixture sample required to store 5.6 kg of usable hydrogen gas. Starting from an empty tank storing hydrogen gas at 77 K and 100 bar, the reduction in external volume is shown for MOF-5(2349):MOF-5(808), 7:1 mixture sample (at 0.40 g/cm^3 and 0.45 g/cm^3 without performance loss) to the system.

storage system. The system assumptions include a baseline multilayer vacuum insulation (MLVI) thickness of 23 mm and 3/8 in. liquid N_2 channels to reduce the type-1 tank temperature during fueling. The initial system model capacity prediction is based on a full state and an empty state of 100 bar/77 K and 5 bar/160 K, respectively. The complete set of assumptions and schematics of the HSECoE system adsorbent system model have been published in ref 25. The effects of the improvements on the system-level volumetric capacity from the 7:1 mixture is depicted in the Figure 5 waterfall chart. The system engineering improvements include optimization of the vacuum insulation (10 mm), reduction of the N_2 channel diameter (1/4"), and SS type 1 tank. Controlling crystal size and use of bimodal distribution of MOF-5 in tandem with system optimization leads to a large decrease in the external volume of about 109 L and exhibits a 30.5 g/L volumetric capacity, sufficient to surpass the 25 g/L volumetric capacity of a typical 700 bar compressed storage system and exceed the DOE 2020 target for volumetric capacity (30 g/L). Similarly impressive results are obtained with MOF-5-O$_h$(600) of a single size suggesting a pathway for even more dramatic improved by controlling size distribution in tandem with crystal shape.

CONCLUSIONS

The enhancement of volumetric storage densities of hydrogen storage systems to levels required for automotive applications is a longstanding problem that particularly plagues physical adsorbents. Although compaction of MOFs has been extensively investigated, the challenge of performance erosion as single crystal densities are approached is universally observed. Here, the ability to achieve high volumetric storage densities (75% of single crystal density) without substantial degradation is achieved. A key to success is the use of crystals with a bimodal size distribution or octahedral morphology sample that can fill space efficiently within a bed and can be compacted with minimal structural damage. A complementary approach based on morphology engineering is also shown to be promising and relies on face-selective inhibition of crystal

https://doi.org/10.1021/jacs.1c04926
J. Am. Chem. Soc. 2021, 143, 10727−10734

growth to induce noncubic morphologies. The principles developed here are fully applicable to the large class of cubic MOF sorbents currently being considered in areas as diverse batteries, carbon capture, separations, and fuel gas storage.

EXPERIMENTAL SECTION

Materials. Terephthalic acid (H_2BDC, 98.0%), 1,3,5-tris(4-carboxyphenyl)benzene (H_3BTB, ≥ 98%), oxalic acid (≥99.0%), malonic acid (99%), succinic acid (≥99.0%), glutaric acid (99%), adipic acid (99.5%), and suberic acid (98%) were purchased from Sigma-Aldrich. 1,3,5-Benzenetricarboxylic acid (≥98%) *N*,*N*-dimethylformamide (DMF, ACS grade), methylene chloride (DCM, HPLC grade, 99.9%), and zinc nitrate hexahydrate ($Zn(NO_3)_2{\cdot}6H_2O$, ACS grade) were purchased from Fisher Scientific. *N*,*N*-Diethylformamide (DEF, 99.0%) was purchased from Acros Organics. [1,1′-biphenyl]-3,4′,5-tricarboxylic acid,[26] 1 2,4,6-tris(4-carboxyphenyl)-aniline (NH_2−H_3BTB, H_3L),[26] 5′-((3,5-dicarboxyphenyl)ethynyl)-[1,1′:3′,1″-terphenyl]-4,4″-dicarboxylic acid (H_4L),[27] and 5′-(4-carboxyphenyl)-[1,1′:3′,1″-terphenyl]-3,4″,5-tricarboxylic acid (H_4L)[28] were synthesized according to the literature procedure.

ASSOCIATED CONTENT

Supporting Information

The Supporting Information is available free of charge at https://pubs.acs.org/doi/10.1021/jacs.1c04926.

The optimized synthesis conditions, solvent exchange and activation procedure, packing density, and compaction measurements protocols(PDF)

AUTHOR INFORMATION

Corresponding Author

Adam J. Matzger − *Department of Chemistry, University of Michigan, Ann Arbor, Michigan 48109, United States; Macromolecular Science and Engineering Program, University of Michigan, Ann Arbor, Michigan 48109, United States;* orcid.org/0000-0002-4926-2752; Email: matzger@umich.edu

Authors

Kuthuru Suresh − *Department of Chemistry, University of Michigan, Ann Arbor, Michigan 48109, United States;* orcid.org/0000-0002-5130-8879

Darpandeep Aulakh − *Department of Chemistry, University of Michigan, Ann Arbor, Michigan 48109, United States;* orcid.org/0000-0002-3082-7709

Justin Purewal − *Ford Motor Company, Research and Advanced Engineering, Dearborn, Michigan 48121, United States*

Donald J. Siegel − *Mechanical Engineering Department, Materials Science & Engineering, Applied Physics Program, and University of Michigan Energy Institute, University of Michigan, Ann Arbor, Michigan 48109, United States;* orcid.org/0000-0001-7913-2513

Mike Veenstra − *Ford Motor Company, Research and Advanced Engineering, Dearborn, Michigan 48121, United States*

Complete contact information is available at: https://pubs.acs.org/10.1021/jacs.1c04926

Notes

The authors declare no competing financial interest.

ACKNOWLEDGMENTS

Financial support for this study was provided by the US Department of Energy, Office of Energy Efficiency and Renewable Energy, Grant no. DE-EE0007046.

REFERENCES

(1) He, T.; Pachfule, P.; Wu, H.; Xu, Q.; Chen, P. Hydrogen carriers. *Nat. Rev. Mater.* **2016**, *1* (12), 1−17.

(2) Li, G.; Kobayashi, H.; Taylor, J. M.; Ikeda, R.; Kubota, Y.; Kato, K.; Takata, M.; Yamamoto, T.; Toh, S.; Matsumura, S.; Kitagawa, H. Hydrogen Storage in Pd Nanocrystals Covered with a Metal-Organic Framework. *Nat. Mater.* **2014**, *13* (8), 802−806.

(3) Barthelemy, H.; Weber, M.; Barbier, F. Hydrogen Storage: Recent Improvements and Industrial Perspectives. *Int. J. Hydrogen Energy* **2017**, *42*, 7254−7262.

(4) Zhang, X.; Leng, Z.; Gao, M.; Hu, J.; Du, F.; Yao, J.; Pan, H.; Liu, Y. Enhanced hydrogen storage properties of MgH_2 catalyzed with carbon-supported nanocrystalline TiO_2. *J. Power Sources* **2018**, *398*, 183−192.

(5) Yang, J.; Sudik, A.; Wolverton, C.; Siegel, D. J. High capacity hydrogen storage materials: attributes for automotive applications and techniques for materials discovery. *Chem. Soc. Rev.* **2010**, *39* (2), 656−675.

(6) Veenstra, M.; Yang, J.; Siegel, D. J.; Ming, Y. Ford/BASF-SE/UM Activities in Support of the Hydrogen Storage Engineering Center of Excellence. https://www.hydrogen.energy.gov/pdfs/progress13/iv_b_7_veenstra_2013.pdf (accessed 2020-09−03), United States Department of Energy, *Hydrogen and Fuel Cells Program 2014 Annual Merit Review Proceedings: Project ST010*, USA, 2013.

(7) Rosi, N. L. Hydrogen storage in microporous metal-organic frameworks. *Science* **2003**, *300*, 1127−1129.

(8) Song, C.; Wang, P.; Makse, H. A. A phase diagram for jammed matter. *Nature* **2008**, *453*, 629−632.

(9) Jaoshvili, A.; Esakia, A.; Porrati, M.; Chaikin, P. M. Experiments on the random packing of tetrahedral dice. *Phys. Rev. Lett.* **2010**, *104* (18), 185501.

(10) Li, H.; Eddaoudi, M.; O'Keeffe, M.; Yaghi, O. M. Design and synthesis of an exceptionally stable and highly porous metal-organic framework. *Nature* **1999**, *402*, 276−279.

(11) Ahmed, A.; Seth, S.; Purewal, J.; Wong-Foy, A. G.; Veenstra, M.; Matzger, A. J.; Siegel, D. J. Exceptional hydrogen storage achieved by screening nearly half a million metal-organic frameworks. *Nat. Commun.* **2019**, *10* (1), 1568.

(12) DeSantis, D.; Mason, J. A.; James, B. D.; Houchins, C.; Long, J. R.; Veenstra, M. *Energy Fuels* **2017**, *31*, 2024−2032.

(13) Rowsell, J. L. C.; Yaghi, O. M. Strategies for hydrogen storage in metalorganic frameworks. *Angew. Chem., Int. Ed.* **2005**, *44*, 4670−4679.

(14) Koh, K.; Van Oosterhout, J. D.; Roy, S.; Wong-Foy, A. G.; Matzger, A. J. Exceptional surface area from coordination copolymers derived from two linear linkers of differing lengths. *Chem. Sci.* **2012**, *3* (8), 2429−2432.

(15) Koh, K.; Wong-Foy, A. G.; Matzger, A. J. A crystalline mesoporous coordination copolymer with high microporosity. *Angew. Chem., Int. Ed.* **2008**, *47*, 677−680.

(16) Park, T.-H.; Hickman, A. J.; Koh, K.; Martin, S.; Wong-Foy, A. G.; Sanford, M. S.; Matzger, A. J. Highly dispersed Palladium(II) in a defective Metal-Organic Framework: application to C-H activation and functionalization. *J. Am. Chem. Soc.* **2011**, *133* (50), 20138−20141.

(17) Chae, H. K.; Siberio-Pérez, D. Y.; Kim, J.; Go, Y.; Eddaoudi, M.; Matzger, A. J.; O'Keeffe, M.; Yaghi, O. M. A route to high surface area, porosity and inclusion of large molecules in crystals. *Nature* **2004**, *427*, 523−527.

(18) Pang, M.; Cairns, A. J.; Liu, Y.; Belmabkhout, Y.; Zeng, H. C.; Eddaoudi, M. Highly monodisperse MIII-Based soc-MOFs (M = In

and Ga) with cubic and truncated cubic morphologies. *J. Am. Chem. Soc.* **2012**, *134*, 13176−13179.
(19) Umemura, A.; Diring, S.; Furukawa, S.; Uehara, H.; Tsuruoka, T.; Kitagawa, S. Morphology design of porous coordination polymer crystals by coordination modulation. *J. Am. Chem. Soc.* **2011**, *133*, 15506−15513 (2011)..
(20) The choice is somewhat arbitrary. There is no theory to guide optimal selection of a randomly packed bimodal distribution of spheres much less guidance for cuboid particles. However, the use of a relatively small mass fraction of the smaller radius particle is established in spherical systems: Schmidt, J.; Parteli, E. J. R.; Uhlmann, N.; Wörlein, N.; Wirth, K.-E.; Pöschel, T.; Peukert, W. Packings of micron-sized spherical particles -Insights from bulk density determination, X-ray microtomography and discrete element simulations. *Adv. Powder Technol.* **2020**, *31*, 2293−2304. Farra, R. S.; Groot, R. D. Close packing density of polydisperse hard spheres. *J. Chem. Phys.* **2009**, *131*, 244104 It is certain that further optimization of relative crystal size and mass ratio of the two sizes would further improve volumetric packing..
(21) Mills, L. A.; Sinka, I. C. Effect of particle size and density on the die fill of powders. *Eur. J. Pharm. Biopharm.* **2013**, *84*, 642−652.
(22) Zakhvatayevaa, A.; Zhonga, W.; Makrooa, H. A.; Harea, C.; Wua, C. Y. An experimental study of die filling of pharmaceutical powders using a rotary die filling system. *Int. J. Pharm.* **2018**, *553*, 84−96.
(23) Purewal, J.; Liu, D.; Yang, J.; Sudik, A.; Siegel, D. J.; Maurer, S.; Müller, U. Increased volumetric hydrogen uptake of MOF-5 by powder densification. *Int. J. Hydrogen Energy* **2012**, *37*, 2723−2727.
(24) Lock, N.; Wu, Y.; Christensen, M.; Cameron, L. J.; Peterson, V. K.; Bridgeman, A. J.; Kepert, C. J.; Iversen, B. B. Elucidating negative thermal expansion in MOF-5. *J. Phys. Chem. C* **2010**, *114*, 16181−16186.
(25) Purewal, J.; Veenstra, M.; Tamburello, D.; Ahmed, A.; Matzger, A. J.; Wong-Foy, A. G.; Seth, S.; Liu, Y.; Siegel, D. J. Estimation of system-level hydrogen storage for metal-organic frameworks with high volumetric storage density. *Int. J. Hydrogen Energy* **2019**, *44* (29), 15135−15145.
(26) Dutta, A.; Koh, K.; Wong-Foy, A. G.; Matzger, A. J. Porous solids arising from synergistic and competing modes of assembly: combining coordination chemistry and covalent bond formation. *Angew. Chem., Int. Ed.* **2015**, *54*, 3983−3987.
(27) Cai, J.; Rao, X.; He, Y.; Yu, J.; Wu, C.; Zhou, W.; Yildirim, T.; Chen, B.; Qian, G. A highly porous NbO type metal-organic framework constructed from an expanded tetracarboxylate. *Chem. Commun.* **2014**, *50*, 1552−1554.
(28) Schnobrich, J. K.; Lebel, O.; Cychosz, K. A.; Dailly, A.; Wong-Foy, A. G.; Matzger, A. J. Linker-directed vertex desymmetrization for the production of coordination polymers with high porosity. *J. Am. Chem. Soc.* **2010**, *132*, 13941−13948.

https://doi.org/10.1021/jacs.1c04926
J. Am. Chem. Soc. 2021, 143, 10727−10734